Fast Backprojection Algorithm for UWB Bistatic SAR

Viet T. Vu, Thomas K. Sjögren and Mats I. Pettersson
Blekinge Institute of Technology (BTH)
Campus Gräsvik, 37179 Karlskorna, Sweden
Email: viet.thuy.vu@.bth.se, thomas.sjogren@bth.se, mats.pettersson@bth.se

***Abstract*— The paper introduces an algorithm for Ultrawideband Ultrawidebeam (UWB) bistatic Synthetic Aperture Radar (SAR). The algorithm works in time-domain and therefore inherits time-domain characteristics such as unlimited scene size, local processing and manageable motion compensation. The proposed algorithm is not limited by any configuration of bistatic SAR. The algorithm processes the UWB bistatic SAR data on a subaperture and subimage basis. This means, instead of backprojecting directly the SAR data to a ground image plane, the algorithm handles the data in two stages: beam forming and local backprojection. The algorithm is named Bistatic Fast Backprojection (BiFBP) and has been tested successfully with the simulated UWB bistatic SAR data.**

I. Introduction

Synthetic Aperture Radar (SAR) plays an important role in geoscience and remote sensing applications. The ability to effectively operate in severe weather conditions is a major advantage of SAR in comparison to other sensor systems. Based on signal bandwidth and antenna beamwidth, SAR systems can be categorized into two groups: Narrowband Narrowbeam(NB) and Ultrawideband Ultrawidebeam(UWB). UWB SAR systems are systems that can offer very high resolution imaging in azimuth and range simultaneously. On the other hand, SAR systems can also be classified by mono- and bistatic if the positions of transmitter and receiver are taken into account. Monostatic SAR is interpreted as SAR systems utilizing co-located transmitter and receiver while bistatic SAR refers to SAR systems whose transmitter and receiver(s) are separated. The benefits of bistatic SAR can be summarized as follows. The possibility to avoid jammers or RFI sources of bistatic SAR seems to be higher than that of monostatic SAR illuminating the same ground scene. Processing SAR data normally requires much effort and may only be performed at ground stations. This can be easily handled with the flexibility in deploying receiver(s) of bistatic SAR. With multiple deployed receivers, an object or a group of objects can be observed at different angles with bistatic SAR. This enhances the classification ability of the object(s). From a system designer's point of view, the design of bistatic SAR is more flexible than of monostatic SAR and the cost to build a bistatic SAR can therefore be minimized.

Due to unique advantages of bistatic SAR, there have been a large number of researches on this topic. Many research works have focused on modifying the currently used monostatic SAR algorithms to process bistatic SAR data where frequency-domain algorithms such as Range Doppler (RD), Range Migration (RM) and Chirp Scaling (CS) receive a great interest. In [1], a discussion on bistatic SAR processing using RD is presented. However, the modified algorithm works only with the azimuth-invariant bistatic configuration where the flight tracks of the transmitter and receiver platforms are parallel and the velocities of these platforms must be identical. Such requirements are not always satisfied in reality, especially for UWB SAR systems that normally require long integration time to handle azimuth focusing. The long integration time causes large range migration and big motion error. For this reason, frequency-domain algorithms are not recommended for UWB SAR data processing [2]. Such processing usually relies on time-domain algorithms, for example Global Backprojection (GBP) [3]. Developing new time-domain algorithms for UWB bistatic SAR is therefore desired.

Although GBP may be used directly for bistatic SAR without any modification, the number of operations required by GBP is relatively high compared to the frequency-domain algorithms. However, there exist fast time-domain algorithms whose computational cost is quite similar to that of frequency-domain algorithms. Extending time-domain monostatic SAR algorithms to bistactic cases seems to be a milestone in UWB bistatic SAR data processing. An attempt to apply Fast Factorized Backprojection (FFBP) to bistatic SAR with retained computational performance is presented in [4]. The data collected by the bistatic SAR system build on SETHI and LORA is experimented with the FFBP.

The objective of this paper is to introduce a fast time-domain algorithm to process UWB bistatic SAR data. The name of Bistatic Fast Backprojection (BiFBP) is assigned to this algorithm. The algorithm inherits the time-domain characteristics and is not limited by any bistatic SAR configuration, i.e. there is no requirement for velocities, flight tracks or flight altitudes of platforms. The proposed algorithm processes the UWB bistatic SAR data on the subaperture and/or subimage basis to reduce the computational load significantly.

The paper is organized as follows. Section 2 reviews the GBP algorithm and the applicability of this algorithm to bistatic UWB SAR is examined. The fast time-domain algorithm for bistatic UWB SAR is presented in Section 3. The algorithm is then tested and evaluated with simulated UWB bistatic SAR data. Simulation results are given in Section 4. Section 5 provides the conclusions.

978-1-4244-8902-2/11/$26.00 ©2011 IEEE

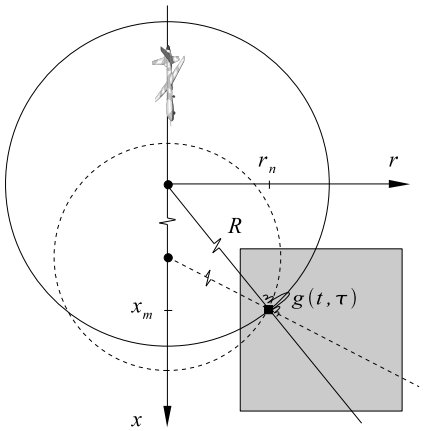

Fig. 1. An illustration of GBP for mono-static SAR and the corresponding iso-ranges at two different time locations. The backprojection of radar echo into a range plane (x, r).

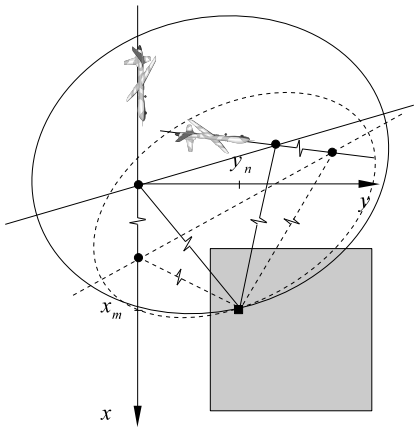

Fig. 2. An illustration of GBP for bistatic SAR and the corresponding iso-ranges at two different time locations. The backprojection of radar echo into a ground plane (x, y).

II. GBP FOR MONO- AND BISTATIC UWB SAR

The GBP algorithm [3] is interpreted as a linear and direct transformation process from radar echo into a complex SAR image. GBP was developed in 1980's and recognized to be one among imaging algorithms which can offer high SAR image quality. For mono-static SAR, the superposition of backprojected radar echo to reconstruct the imaged scene on the slant range plane (x_m, r_n) is mathematically represented by the integral

$$h(x_m, r_n) = \int_{-\frac{t_i}{2}}^{+\frac{t_i}{2}} g(v_{pl}t, R)\, dt \tag{1}$$

where t_i is the integration time and v_{pl} denotes the speed of the platform and

$$R = \sqrt{(v_{pl}t - x_m)^2 + r_n^2} \tag{2}$$

The range-compressed radar echoes are given by $g(t, \tau)$ where t and τ indicate azimuth-time (slow-time) and range time (fast-time), respectively. Figure 1 illustrates the backprojection of radar echo into a range plane (x, r). As shown, the backprojection of GBP for mono-static SAR is performed over the spherical mapping. The center of the circle is determined by the aperture position of the platform and the radius is given by the range R. The SAR image pixel (x_m, r_n) and other pixels, which have the same range R given by (2), i.e. crossed by the solid circle in Fig. 1, are assigned a value of a range-compressed radar echo sample corresponding to this range.

For bistatic SAR, there are more than one range plane if the flight tracks of the transmitter and receiver platforms are not in a straight line. The imaged scene is therefore recommended to reconstruct on the ground plane instead of the range plane to simplify the range calculation. An illustration of GBP for bistatic SAR is given in Fig. 2. The backprojection of GBP for bistatic SAR is performed over the elliptical mapping. The foci of the ellipse are determined by the aperture positions of the transmitter and receiver platforms at a time instance. The major axis is defined by the line connected the aperture positions of transmitter and receiver platforms together. The range R indicates the major diameter of the ellipse. The mathematic expression of the bistatic GBP (BiGBP) is given by

$$h(x_m, y_n) = \int_{-\frac{t_i}{2}}^{+\frac{t_i}{2}} g(v_t t, v_r t, R)\, dt \tag{3}$$

where v_t and v_r denote the speed of the transmitter and receiver platforms, respectively. The range R depends on the movements of the platform and is now estimated by

$$\begin{aligned} R &= \sqrt{(v_{t,x}t - x_m)^2 + (v_{t,y}t - y_n)^2 + h_t^2} + \\ &\quad \sqrt{(v_{r,x}t - x_m)^2 + (v_{r,y}t - y_n)^2 + h_r^2} \end{aligned} \tag{4}$$

where the subscripts x and y denote the speed components. The SAR image pixel (x_m, y_n) and other pixels, which have the same range R given by (4), i.e. crossed by the solid ellipse in Fig. 2, are assigned a value of a range-compressed radar echo sample corresponding to this range.

In both mono- and bistatic GBP (BiGBP), the ranges R between all aperture positions and all SAR image pixels are need to be calculated. This makes GBP inefficient in terms of processing time. However, this is exchanged by high quality SAR images offered by GBP and the independence of GBP on bistatic configuration. The range calculation based on each aperture position in GBP also means that the motion errors are compensated automatically. The scene size illuminated by a SAR system can be seen to be unlimited and depends strongly on the antenna beamwidth, integration time, flight attitude, radiated power, Pulse Repetition Frequency (PRF) of that SAR system. Also, the scene imaged by GBP can be selected from small area to the whole illuminated scene.

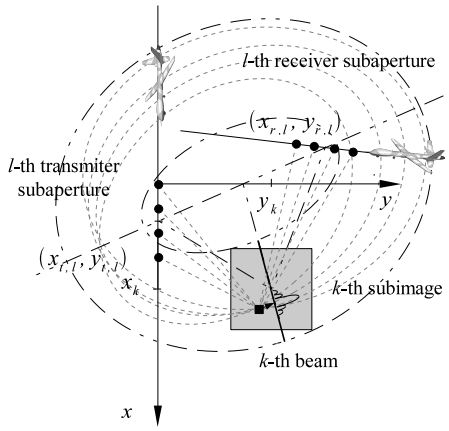

Fig. 3. Beam forming in BiFBP. Beam forming is a superposition of the radar echo belonging to the $l-$th transmitter and receiver subapertures.

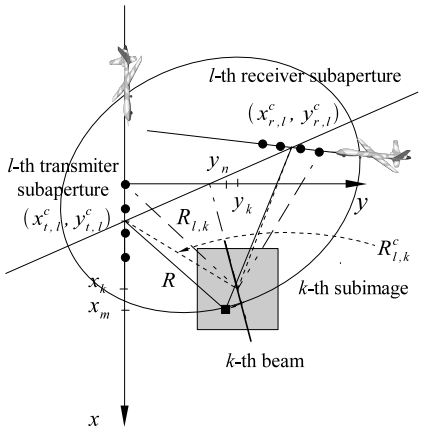

Fig. 4. Local backprojection in BiFBP. The backprojection is performed over the elliptical mapping.

III. Bistatic Fast Backprojection UWB SAR

A fast time-domain algorithm, named Bistatic Fast Backprojection (BiFBP), is introduced in this section. Similar to BiGBP, the imaged scene is also supposed to be reconstructed on the ground plane instead of the range plane to simplify range calculation. The algorithm processes SAR data on a subaperture and subimage basis, i.e. local processing. Thus, the full imaged scene is segmented into K subimages while the complete transmitter and receiver apertures are split into L subapertures.

In the beam forming stage, all radar echo belonging to the $l-$th subapertures are first shifted with respect to the center of the $k-$th subimage and then superposed to form the $k-$th beam. As illustrated in Fig. 3, this superposition can be interpreted as the projection of the data samples into the beam samples over an elliptical mapping. The beam forming procedure can be mathematically represented by

$$b\left(v_t t_l, v_r t_l, \mathrm{c}\tau - R_{l,k}\right) = \int_{t_l-\frac{t_s}{2}}^{t_l+\frac{t_s}{2}} g\left(v_t t, v_r t, \mathrm{c}\tau - R_{l,k}\right) dt \quad (5)$$

where t_l denotes the time instant corresponding to the $l-$th centers of the subapertures, t_s the integration time, and c is the speed of light. The distance from an aperture position belong to the $l-$th transmitter subaperture via the center of the $k-$th subimage to the coresponding aperture position belong to the $l-$th receiver subaperture $R_{l,k}$ is estimated by

$$\begin{aligned} R_{l,k} &= \sqrt{\left(x_{t,l}-x_k\right)^2+\left(y_{t,l}-y_k\right)^2+h_t^2}+ \\ &\quad \sqrt{\left(y_{r,l}-x_k\right)^2+\left(y_{r,l}-y_k\right)^2+h_r^2} \end{aligned} \quad (6)$$

where (x_k, y_k) are the coordinates of the center of the $k-$th subimage on the ground plane. Aperture positions belonging to the $l-$th subapertures are denoted by $(x_{t,l}, y_{t,l})$ and $(x_{t,r}, y_{t,r})$. The number of beam samples $b\left(t_l, R - R_{l,k}\right)$ is selected to be just enough to cover the whole subimage. As demonstrated in Fig. 3, this optimum selection of the beam length is limited by two dotted-dashed ellipses.

The $k-$th subimage is then backprojected from the $k-$th beam in the backprojection stage. The backprojection is performed over an elliptical mapping. The $l-$th centers of the transmitter and receiver subapertures determine the foci of the ellipse. The major axis is defined by the line between the two foci. The major diameter of the ellipse is given by a range R

$$\begin{aligned} R &= \sqrt{\left(x_{t,l}^c-x_m\right)^2+\left(y_{t,l}^c-y_n\right)^2+h_t^2}+ \\ &\quad \sqrt{\left(x_{r,l}^c-x_m\right)^2+\left(y_{r,l}^c-y_n\right)^2+h_r^2} \end{aligned} \quad (7)$$

where $\left(x_{t,l}^c, y_{t,l}^c\right)$ and $\left(x_{r,l}^c, y_{r,l}^c\right)$ are the centers of the $l-$th subapertures. As shown in Fig. 4, the SAR image pixel (x_m, y_n) and other pixels, which have the same range R, i.e. crossed by the solid ellipse, belonging to the $k-$ th subimage are assigned a value of the $k-$ th beam samples which differs from the center of the $k-$ th beam a distance of $R - R_{l,k}^c$

$$h_k\left(x_m, y_n\right) = \sum_{l=1}^{L} b\left(v_t t_l, v_r t_l, R - R_{l,k}^c\right) \quad (8)$$

where

$$\begin{aligned} R_{l,k}^c &= \sqrt{\left(x_{t,l}^c-x_k\right)^2+\left(y_{t,l}^c-y_k\right)^2+h_t^2}+ \\ &\quad \sqrt{\left(x_{r,l}^c-x_k\right)^2+\left(y_{r,l}^c-y_k\right)^2+h_r^2} \end{aligned} \quad (9)$$

This procedure will be repeated for all subapertures. The full SAR image is finally retrieved by a coherent combination of all subimages

$$\begin{aligned} &h\left(x_m, y_n\right) = \\ &\bigcup_{k=1}^{K}\sum_{l=1}^{L}\int_{t_l-\frac{t_s}{2}}^{t_l+\frac{t_s}{2}} g\left(v_t t, v_r t, \mathrm{c}\tau - R_{l,k}^c + R - R_{l,k}\right) dt \end{aligned} \quad (10)$$

Equation (11) is the mathematical representation of BiFBP.

TABLE I

PARAMETERS OF TRANSMITTER AND RECEIVER PLATFORMS.

Parameter	CARABAS-II (transmitter)	(receiver)
The highest frequency processed	82 MHz	
The lowest frequency processed	22 MHz	
Platform speed v_{pl}	126 m/s	130 m/s
Aperture step	0.9375 m	0.9673 m
Flight altitude	3700 m	2900 m
Minimum range r_0	5900 m	3000 m
PRF	137 Hz	

IV. SIMULATION RESULTS AND EVALUATIONS

In this section, we present some simulation results to test and evaluate the proposed algorithm BiFBP. The simulated bistatic SAR system is based on the CARABAS-II parameters [5] and the motion parameters of LORA [6]. The main parameters used in the simulations are summarized in Table I. The transmitter is carried by CARABAS-II and the receiver by another platform. An angle of 60^{o} formed by two flight tracks is randomly selected. The number of considered aperture position is 4096 corresponding to an integration angle of 35^{o} with respect to the transmitter platform. The ground scene is simulated by a number of point-like scatters spaced equally. The reconstructed SAR scene is assumed to be limited by 256 m$\times$256 m and the image pixel is chosen by 1 m$\times$1 m.

Fig. 5.a shows the simulated SAR scene which is reconstructed with BiGBP. In this SAR image, the scatters are well focused and appear as the point targets. Their general features, i.e. point-like scattering, orthogonal and non-orthogonal sidelobes, are very similar to monostatic SAR. However, the point targets are inclined with an angle. This inclination is supposed to be dependent of the motion parameters of the transmitter and receiver platforms. The SAR image processed with BiGBP is seen as the reference to evaluate BiFBP's performance.

The same SAR scene is again reconstructed with BiFBP and given in Fig. 5.b. In this example, the number of subapertures $L = 64$ and subimages $K = 256$ are selected. The subaperture length is then calculated to be 64×0.9375 m while the subimage size is given by 16 m$\times$16 m. The phase error with this selection can be shown to be about $\pi/20$. The result shows that BiFBP works perfectly with UWB bistatic SAR. There is no clear difference between the SAR images processed by BiGBP and BiFBP. The computational cost of BiFBP is supposed to be similar to that of FBP for monostatic cases.

V. CONCLUSION

In this study, the ability to use GBP for bistatic SAR is examined. A fast time-domain algorithm named BiFBP is presented. The algorithm is aimed at UWB bistatic SAR systems. The algorithm inherits the time-domain characteristics and is not limited by any bistatic SAR configuration. The algorithm is tested with the simulated data based on the CARABAS-II parameters and the motion parameters of LORA.

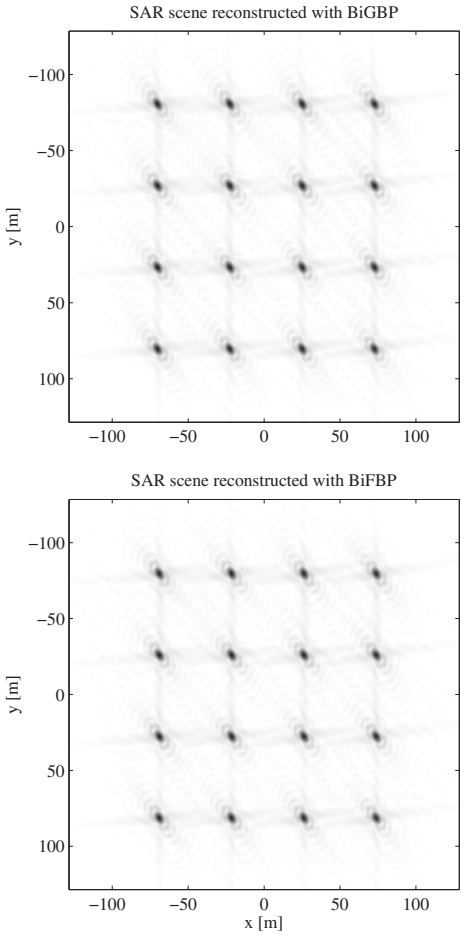

Fig. 5. The UWB bistatic SAR image of the ground scene. (a) The SAR data is processed with BiGBP, (b) The SAR data is processed with BiFBP.

ACKNOWLEDGMENT

The authors would like to thank the KK-Foundation for the financial support in this research project, the Swedish Defence Research Agency, Saab Bofors Dynamics, Saab Electronic Defence Systems and RUAG Space for their cooperation.

REFERENCES

[1] Yew Lam Neo, F.H. Wong, and I.G. Cumming, "Processing of azimuth-invariant bistatic SAR data using the range doppler algorithm," *IEEE Trans. Geosci. Remote Sensing*, vol. 46, no. 1, pp. 14–21, 2008.

[2] V. T. Vu, T. K. Sjögren, and M. I. Pettersson, "A comparison between fast factorized backprojection and frequency-domain algorithms in UWB low frequency SAR," in *Proc. IEEE IGARSS'2008*, Boston, MA, Jul. 2008, pp. 1293–1296.

[3] L. E. Andersson, "On the determination of a function from spherical averages," *SIAM Journal on Mathematical Analysis*, vol. 19, no. 1, pp. 214–232, 1988.

[4] L. M. H. Ulander, P.-O. Frölind, A. Gustavsson, D. Murdin, and G. Stenström, "Fast factorized back-projection for bistatic SAR processing," in *Proc. IEEE EUSAR 2010*, Aachen, Germany, June 2010, pp. 4(p).

[5] A. Gustavsson, L. M. H. Ulander, B. H. Flood, P.-O. Frölind, H. Hellsten, T. Jonsson, B. Larsson, and G. Stenstrom, "Development and operation of an airborne VHF SAR system-lessons learned," in *Proc. IEEE IGARSS'98*, vol. 1, Seattle, WA, Jul. 1998, pp. 458–462.

[6] H. Hellsten and L. M. H. Ulander, "Airborne array aperture UWB UHF radar-motivation and system considerations," *IEEE Aerosp. Electron. Syst. Mag.*, vol. 15, no. 5, pp. 35–45, 2000.